Engineered Science

REVIEW PAPER View Article Online

Recent Progress on the Metacompoistes with Carbonaceous Fillers

Haikun Wu, Xiaoshuai Huang and Lei Qian*

Different from common "*Metamaterials*", "*Metacomposites*" are used to describe random nanocomposites with negative permittivity, which is determined by controlling their microstructures and compositions. Metacomposites with unique negative permittivity show potential applications in superconductors, wave filters, capacitors, electromagnetic interference shielding or absorbing and other fields. In this review, Drude model, Lorentz model and "double nano wires" model used to analyze negative permittivity were discussed. Preparation, properties and mechanism of negative permittivity from metacomposites in corporation of carbon nanomaterials as fillers were reviewed and analyzed. Besides, the applications of metacomposites in the field of electromagnetic wave absorption and improving the performance of the antenna were also discussed.

Keywords: Metacomposites; Carbon nanomaterials; Negative permittivity

Received 21st April 2018, Accepted 7th May 2018

DOI: 10.30919/es8d656

1. Introduction

In recent years, metamaterials whose permittivity and permeability are negative have drawn increasing attention. In the metamaterials, the Poynting vector determined by macroscopic electric field (E) and magnetic field (H) is opposite to the wave vector (k), so the triad of vectors containing E, H and k is left-handed.[1,2] As a result, the metamaterials are also called left-handed media.[3] These special materials exhibit many novel electromagnetic properties such as negative refractive index, inverse Cerenkov radiation, inverse Doppler effect and so on.[4–10] Metamaterials show potential applications in the area of magnetic resonance imaging, wireless power transfer, perfect lens and invisible cloak, etc.[11–14]

Generally, metamaterials do not exist in natural materials and instead are artificially fabricated with special structures.[15] Recently, Guo et al.[16,17] used the term "*metacomposites*" to describe random nanocomposites with negative permittivity. Compared with metamaterials, metacomposites show many advantages and differences. For example, the bandwidth of negative permittivity in metamaterials is narrow, which is determined by the periodic artificial structures.[18] Besides, the negative permittivity in metamaterials is controlled by the size of periodic unit structures, so it is difficult to achieve negative index parameters in the high frequency regions due to the size effect.[19] The fabrication of artificial periodic unit structures is complex, so negative index parameters are not easy to be tuned by changing the size of unit structures in metamaterials.[20] However, the negative permittivity in the metacomposites is determined by their microstructures and compositions rather than periodic unit structures.[20] As a result, it is easier to adjust the negative permittivity in metacomposites by controlling compositions and microstructures.[21] Additionally, preparation of metacomposites provides a new method and route to design and manufacture metamaterials.[22,23]

Although there are many reviews about metamaterials, the review about metacomposites from carbon nanostructures has not been reported. In this review, the Drude model, Lorentz model and double nano wires model which are used to analyze the mechanism of negative permittivity are introduced in detail. Besides, current research on metacomposites with graphene, carbon nanotubes, carbon nanofibers and amorphous carbon as fillers is also discussed.

2. The model for the negative permittivity

2.1. Negative permittivity fitted with Drude model

At first, the Drude model is mainly used to analyze the negative permittivity in metal-based negative refractive index materials. The negative perrmittivity in these materials is observed due to the plasma-like resonance of free electrons on the metal surface.[24,25]

In the Drude model, metals are considered as classical gas of electrons which perform diffusive motion. Assuming that an average relaxation time τ governing the relaxation of the system to equilibrium exists in the Drude model, the state with average momentum is

Key Laboratory for Liquid-Solid Structural Evolution and Processing of Materials (Ministry of Education), Shandong University, 17923 Jingshi Road, Jinan 250061, China. E-mail: qleric@sdu.edu.cn

zero (‹**p**› = 0) when an external field E is removed. The rate equation is expressed as:[26]

$$\frac{\mathrm{d}\langle \mathrm{p}\rangle}{\mathrm{dt}} = -\frac{\langle \mathrm{p}\rangle}{\tau} \tag{1}$$

If an external electric field E is applied, the equation of motion can be expressed as:[26]

$$\frac{\mathrm{d}\langle \mathrm{p}\rangle}{\mathrm{dt}} = -\frac{\langle \mathrm{p}\rangle}{\tau} - e\mathrm{E} \tag{2}$$

where e is the electronic charge. The current density is given by the formula:[26]

$$\mathrm{J} = -\frac{\mathrm{Nep}}{\mathrm{m}} \tag{3}$$

where, J is the current density, m is the carrier mass, N is the density of charge carriers. When d‹**p**›/dt = 0, the dc conductivity (σ_{dc}) is given:[26]

$$\sigma_{dc} = \frac{J}{E} = \frac{Ne^2\tau}{m} = \frac{1}{4\pi}\omega_p^2\tau \tag{4}$$

where ω_p=($4\pi Ne^2$/m)$^{1/2}$ is the plasma frequency, when an ac field is applied in the form E(t) = E_0 exp(-iωt), according to the equation of motion:[26]

$$\mathrm{m}\frac{\mathrm{d}^2\mathrm{r}}{\mathrm{dt}^2} + \frac{\mathrm{m}}{\tau}\frac{\mathrm{dr}}{\mathrm{dt}} = -\mathrm{eE(t)} \tag{5}$$

a complex, frequency dependent conductivity is given:[26]
with the components:[26]

$$\sigma^*(\omega) = \frac{\sigma_{dc}}{1-i\omega\tau} = \frac{Ne^2}{m}\frac{1}{1/\tau - i\omega} = \frac{\omega_p^2}{4\pi}\frac{1}{1/\tau - i\omega} = \sigma_1(\omega) + \mathrm{i}\sigma_2(\omega) \tag{6}$$

$$\sigma_1(\omega) = \frac{\omega_p^2\tau}{4\pi}\frac{1}{1+\omega^2\tau^2} \quad \text{and} \quad \sigma_2(\omega) = \frac{\omega_p^2\tau}{4\pi}\frac{\omega\tau}{1+\omega^2\tau^2} \tag{7}$$

The relationship between the complex dielectric permittivity and conductivity is described as:[26,27]

$$\varepsilon^* = 1 + \frac{4\pi\mathrm{i}}{\omega}\sigma^* \tag{8}$$

According to the equation (6), (7) and (8), the Drude model is described as:[28–31]

$$\begin{aligned}\varepsilon^*(\omega) &= 1 - \frac{\omega_p^2}{\omega(\omega + \mathrm{i}/\tau)} \\ &= \left(1 - \frac{\omega_p^2\tau^2}{1+\omega^2\tau^2}\right) + \mathrm{i}\left(\frac{\omega_p^2\tau}{\omega(1+\omega^2\tau^2)}\right)\end{aligned} \tag{9}$$

And the real part of the permittivity (ε') is expressed as:

$$\varepsilon' = 1 - \frac{\omega_p^2\tau^2}{1+\omega^2\tau^2} \tag{10}$$

From equation (10), it is observed that negative permittivity is obtained when the angular frequency of the applied electromagnetic field ω is lower than the angular plasma frequency ω_{p}, and the permittivity becomes positive if the angular frequency ω exceeds the angular plasma frequency ω_{p}.[32]

2.2. Negative permittivity fitted with Lorentz model

The Lorentz model is also a classical dielectric function model. Lorentz model considers the relaxation, corresponding to the electrons transferring between bands in the material. The Lorentz model has been used for many solid materials including metals and semiconductors.[33]

Under the action of an applied electric field, an electrical medium is able to be polarized, which is described as the dielectric properties. Placing an electrical medium in an applied electric field, the electrical charges move from their average equilibrium positions, causing dielectric polarization (displacement).[1] Due to the polarizability of the molecules and atoms in the dielectric medium, the polarization of materials which show frequency-dependent dielectric properties is less likely to respond to the applied electric field. In an applied electric field, a dipole moment is introduced because of the charge separation of negatively charged electrons and positively charged nuclei in molecules and atoms. The force on the electron is expressed by the Lorentz force (**F**):[1,33]

$$\mathrm{F} = -\mathrm{e}(\mathrm{E} + \upsilon \times \mathrm{H}) \tag{11}$$

where H is the magnetic field, E is the macroscopic electric field, e is the electron charge, and v is the velocity of electrons. Under an action of the elastic restoring force, the electron in a molecule or atom is bound to the equilibrium position. As a result, the equation of electron motion is expressed as eq. (12):[1,33]

$$\mathrm{m}\ddot{\mathrm{r}} + \mathrm{m}\gamma\dot{\mathrm{r}} + \mathrm{m}\omega_0^2\mathrm{r} = -\mathrm{eE}_0\exp(-\mathrm{i}\omega\mathrm{t}) \tag{12}$$

where, m is the mass of the electron, r is the displacement vector, r̈ is the second derivative with respect to t, ṙ is the first derivative

with respect to t, ω (ω=2πf) is the angular frequency of the applied electromagnetic field and f is the frequency of the applied electromagnetic field, ω_0 (ω_0 = 2πf_0) is the resonance angular frequency characterizing the harmonic potential trapping of the electron to the equilibrium position, f_0 is the resonance frequency, γ is the dissipation parameter, t is the time, m$\gamma\dot{\mathbf{r}}$ is the phenomenological damping force on the electron because of all of the inelastic processes.

The displacement of the electron is obtained by using a trial solution: $\mathbf{r}=\mathbf{r_0}\exp(-i\omega t)$ and can be expressed as:[33]

$$\mathrm{r}_0 = \frac{-\mathrm{eE}_0 / \mathrm{m}}{\omega_0^2 - \omega\left(\omega + \mathrm{i}\gamma\right)} \tag{13}$$

Compared with the travelled distance of the electrons, the wavelength of the radiation is larger, so the electrons are more likely to move along a uniform field. As a result, the dipole moment attributed to each electron is expressed as: p=-$e\mathbf{r}$. The polarization (P) is defined as the total dipole moment per unit volume, so it is calculated by the vectorial sum of all the dipoles. If there is one dipole in per molecule and the average number of molecules per unit volume is N, the polarization (P) can be expressed as:[33]

$$\mathrm{P} = \mathrm{Np} = \frac{\mathrm{Ne}^2\mathrm{E} / \mathrm{m}}{\omega_0^2 - \omega\left(\omega + \mathrm{i}\gamma\right)} = \varepsilon_0 \chi_\mathrm{e} \mathrm{E} \tag{14}$$

where, ε_0 is the vacuum permittivity, χ_e is the dielectric susceptibility. The complex dielectric permittivity is expressed as:[33–35]

$$\varepsilon\left(\omega\right) = 1 + \chi_\mathrm{e}\left(\omega\right) = 1 + \frac{\mathrm{Ne}^2 / \mathrm{m}\varepsilon_0}{\omega_0^2 - \omega\left(\omega + \mathrm{i}\gamma\right)} = 1 + \frac{\omega_\mathrm{p}^2}{\omega_0^2 - \omega^2 + \mathrm{i}\Gamma_\mathrm{L}\omega} \tag{15}$$

where, ω_p=(Ne^2/mε_0)$^{1/2}$=(4πNe^2/m*) is the angular plasma frequency, m* is the effective mass of the electron,[1] Γ_L=-1/γ is the damping constant related to the resonance. The equation (15) is called the Lorentz formula. According to the Lorentz model, the real part of the permittivity can be expressed as:[34–37]

$$\varepsilon' = 1 + \frac{\omega_p^2\left(\omega_0^2 - \omega^2\right)}{\left(\omega_0^2 - \omega^2\right)^2 + \omega^2\Gamma_L^2} \tag{16}$$

It is observed from equation (16) that, when ω/ω_0>1 meaning that the frequency of applied electromagnetic field exceeds the resonance frequency, the real part of permittivity becomes negative.

2.3. Negative permittivity fitted with "double nano wires" model

Yao et al.[38] constructed a structure model called "double nano wires" model to analyze the generation mechanism of negative permittivity in the MWCNTs-polyaniline (PANI) metacomposites. They simplified the internal conditions of the composite. For example, they regarded the PANI long chains as some inductors in the PANI. When an alternative electric field was applied, the current phase lagged behind the phase of electric field for π/2 (Figure 1a). The alternating current was considered as an oscillating electric dipole, and the oscillating electric dipole phase lagged behind the current phase for π/2 (Figure 1b). As a result, the oscillating electric dipole phase lagged behind the electric field phase for π, meaning the direction of induced electric field strength E_i (induced charges) was opposite to the direction of electric field strength E_f (free of charge). Due to the multiple effects, the alternating dipoles could form $\sum E_i$. If the sum of $\sum E_i$ and polarization electric field strength E_p (polarization charges) was more than E_f (E_p + E_i > E_f), the negative permittivity appeared in the composite (Figure 1c). That was called the "nano wires" model. In the MWCNTs-PANI composites, MWCNTs and PANI were both regarded as inductors, and these two kinds of inductors were equivalent to double nano wires. The generation mechanism of negative permittivity was similar to above. The researchers proposed that only the MWCNTs which paralleled to or less than 45° the direction of external alternating electric field were considered as inductors generating the alternating current dipoles and alternating current. Due to the low resistance and regular shape of MWCNTs, the nano wires of MWCNTs generated a larger E_i. Furthermore, nano wires of MWCNTs helped PANI produce a larger E_i by improving polarization of alternating current dipoles. As a result, MWCNTs/PANI composites achieved a larger negative permittivity. This is the "double nano wires" model (Figure 2). The resistivity of PANI and MWCNTs-PANI composites increased with the frequency, so the ability of electrons to hop between chains became weak, resulting in the decrease of E_i. As a result, the sum of E_p and E_i decreased and the permittivity increased with the frequency. When the sum of E_p and E_i was less than E_f (E_p + E_i < E_f), the permittivity converted from negative to positive.

3. Current research on metacomposites with carbon nanostructures as nanofillers

Currently, the metacomposites mainly have been produced by combining the functional characteristics of nanofillers with excellent electrical and magnetic properties into matrix.[39–46] Incorporating metallic materials (like alumina and silver) and carbon materials (amorphous carbon, carbon nanotubes, carbon nanofibers and graphene) into matrix is more likely to fabricate metacomposites with negative permittivity, because the negative permittivity behavior is mainly attributed to the plasma oscillation of delocalized electrons in metallic clusters or the dielectric resonance of the polarization.[47–51]

Carbon materials are distinct from metallic materials, because carbon materials like amorphous carbon with zero-dimensional (0D) structure, carbon nanotubes (CNTs) , carbon nanofibers (CNFs)

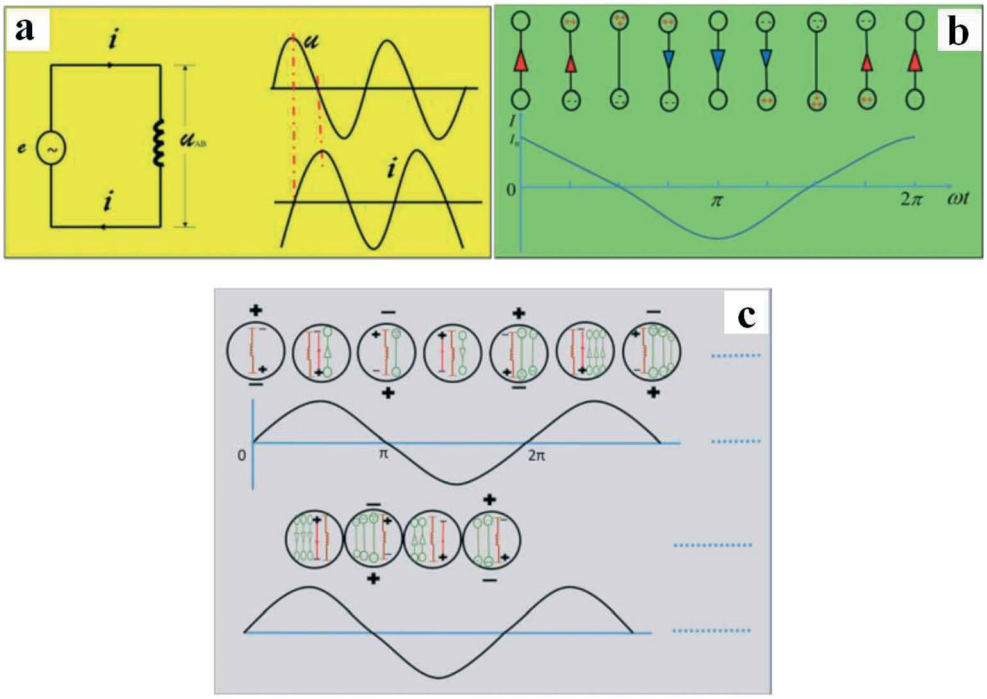

Fig. 1 (a) The phase difference between alternating electric field and alternating current, (b) The phase difference between alternating current dipole and alternating current, (c) The generation of negative permittivity. Reprinted with permission.[38] Copyright 2016, RSC.

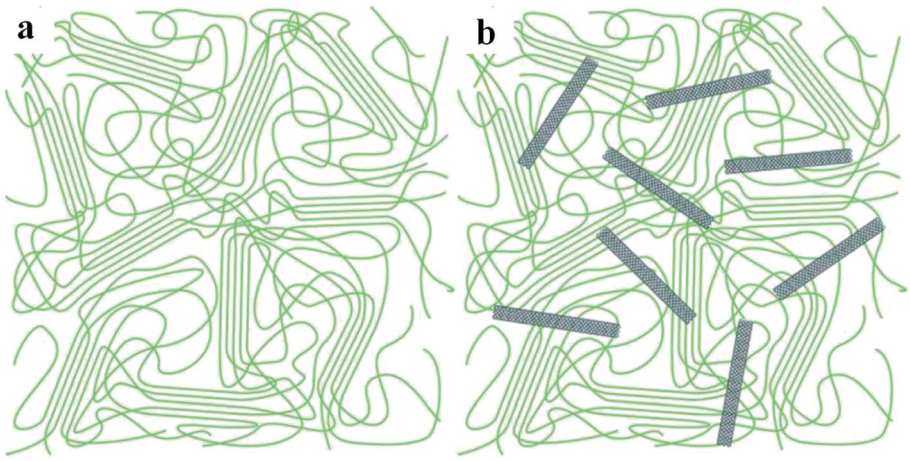

Fig. 2 (a) "nano wires" model of CPA0 (PANI), (b) "double nano wires" model of MWCNTs-PANI composites. Reprinted with permission.[38] Copyright 2016, RSC.

with one-dimensional (1D) structure and graphene (GR) with two-dimensional (2D) always show good electronic mobility, high mechanical stiffness, large specific surface area, good thermal conductivity and other extraordinary properties.[52–55] As a result, these carbon materials used as effective additives are often incorporated into matrix to improve the magnetic, optical, electrochromic, conductive, mechanical and dielectric properties of nanocomposites.[56–59] For instance, the GR-polypyrrole-epoxy composites with enhanced electrical properties,[60] the GR-poly(benzobisoxazole) nanocomposites with high thermal stability,[61] the graphene nanoplatelets (GNPs)-epoxy composites with improved tensile and compressive mechanical properties[62] have been reported.

In metacomposites with metallic materials as nanofillers, the value of negative permittivity is always very high (the magnitude can reach 10^4) due to plasma resonance of free electrons on metal surfaces. So it is difficult to achieve the match between permittivity and permeability. However, the concentration of free electrons on the surface of carbon materials is low compared with metals, so it is expected to realize the weakly negative permittivity in metacomposites with carbon materials as nanofillers.

3.1. Metacomposites with GR as fillers

Our group has observed the negative permittivity fitted with the Lorentz model in the magnetic graphene (FGR)-phenolic resin (PR)

composites.[63] The transition of dielectric constant from positive to negative (75 to -75) was observed in the FGR-PR composites when the FGR content reached 91 vol%. According to the Lorentz model, the negative permittivity appeared when the frequency of applied electromagnetic field exceeded the resonance frequency, and the resonance frequency for FGR91 was about 460 MHz. As a result, the positive was observed when the frequency was lower than 460 MHz and the permittivity became negative when the frequency exceeded 460 MHz for FGR91. Despite the negative permittivity fitted with the Lorentz model, the negative permittivity (-75 to -25) over the whole frequency in FGR98 was consistent with the fitted results from the Drude model.

Yin et al.[64] achieved the negative permittivity from the graphene-alumina (GR-Al_2O_3) composites which were prepared by the spark plasma sintering method. A plasma-like negative permittivity (Figure 3a) was achieved when GR content reached 15.38 and 18.64 wt%, attributing to the fabrication of continuous GR networks (Figure 3c and d). Interestingly, a transition of permittivity from negative to positive (-2000 to 250) was observed in $GR_{15.38}$ and $GR_{18.46}$, which was explained by the LC resonances and agreed well with the Drude model. Besides, the dielectric loss contained the conduction loss and the polarization loss in the GR-Al_2O_3 ceramics, and the ε'' increased with the increasing GR content (Figure 3b).

Zhu et al.[65] prepared the magnetic GR nanocomposites with iron pentacarbonyl as the precursor by a thermal-decomposition method. The researcher observed the negative permittivity at about 3000 Hz when the particle loading increased from 2 to 5 wt%, attributing to the electronic energy dispersion in surface plasmons. Wu et al.[66] have reported the negative permittivity from flexible GR-acrylic polyurethane composites. Due to the good dispersion of GR in acrylic polyurethane matrix, the negative permittivity fitted with Drude model appeared in low GR content (only 3 vol%). And the GR-acrylic polyurethane metacomposites showed good flexibility, extending the applications of metacomposites. Wu et al. [67] have also reported the tunable negative permittivity in the GR-phenolic resin composites.

3.2. Metacomposites with CNTs as fillers

Sun et al.[12] obtained the negative permittivity from the flexible polydimethylsiloxane (PDMS)-multi-walled carbon nanotubes (MWCNTs) membranous nanocomposites with in-situ polymerization process. When the MWCNTs content reached 5 wt%, the negative permittivity with a small value (-25 to 0) was found. And the transmission frequency with permittivity from positive to negative was about 933 MHz. The researchers thought that the negative permittivity was attributed

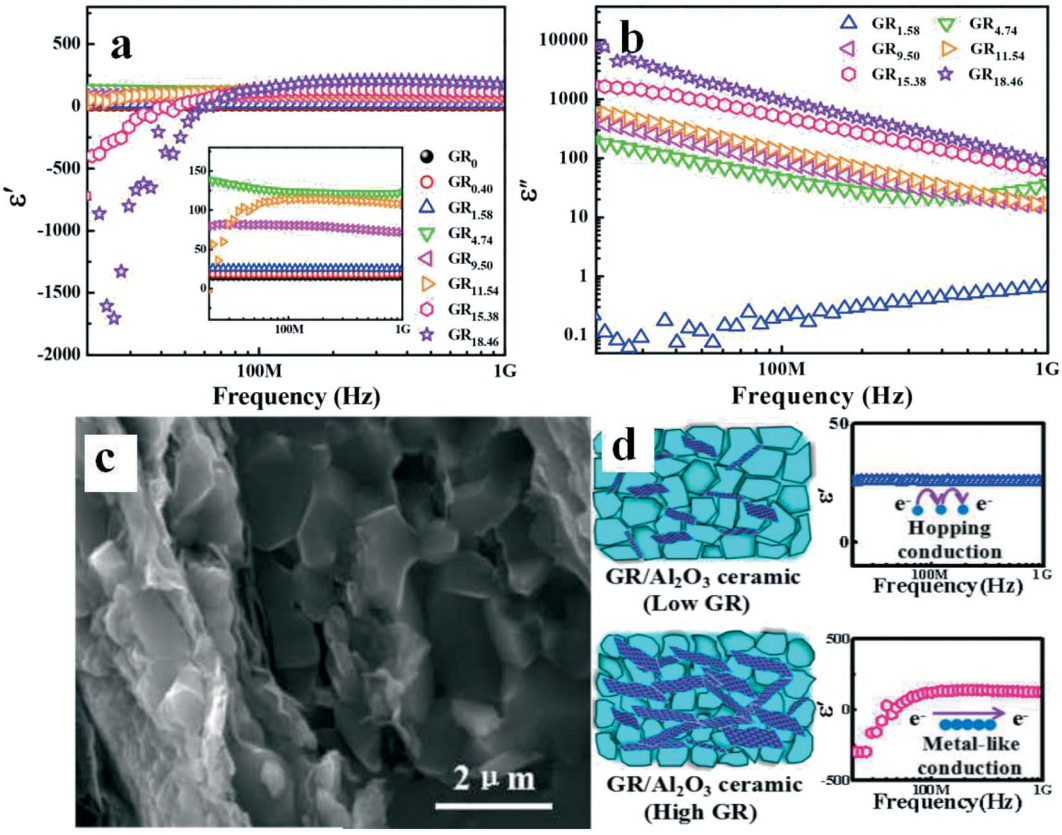

Fig. 3 (a) Frequency dependences of the real permittivity for GR-Al_2O_3 composites with different GR contents, (b) Frequency dependences of the imaginary permittivity for GR-Al_2O_3 composites with different GR contents, (c) FESEM image of the GR-Al_2O_3 composite with GR content of 15.38 wt%, (d) schematic of the mechanism of negative permittivity in the GR-Al_2O_3 composite ceramics. Reprinted with permission. [64] Copyright 2018, ACS.

to a dielectric resonance called the Lorentz model, and the resonance characteristic was due to the huge damping coefficient. [35,68]

Sun et al.[69] prepared the polyimide-multi-wall carbon nanotubes (PI-MWCNTs) composite films via a water-based method with the use of triethylamine (Figure 4). The negative permittivity appeared when MWCNTs content was 8.1 and 8.7 vol%. The negative permittivity increased with the frequency, changed into positive values and then remained about zero in the high frequency region.

3.3. Metacomposites with CNFs as fillers

Zhu et al.[70] achieved negative permittivity in the polymer nanocomposites (PNCs) with CNFs as fillers and two different elastomers (VM1, VM2) as polymer matrix, which were prepared through the solvent-assisted casting method. The researchers observed negative permittivity (-3×10^4 to 0 and -1.8×10^5 to 0) in the 3 wt% CNFs-VM1 PNCs and 5 wt% CNFs-VM1 PNCs before 10^3 Hz. The appearance of negative permittivity resulted from the formation of a continuous conductive network of CNFs when the CNFs loading increased to 3 wt% and 5 wt%. Li et al.[18] have obtained the negative permittivity in the CNFs-polyetherimide (PEI) nanocomposites which were prepared by the solution-processing method. They found that the absolute values of negative permittivity increased with increasing CNFs loading from 1 wt% to 5 wt% in the frequency range of 100 - 3 MHz (Figure 5a). A resonance at 5 kHz was observed and the negative permittivity was attributed to this resonance. In order to prove this, the researchers cut long CNFs by ultrasonic treatment, improving the dispersion of CNFs in the polymer matrix but destroying the continuous CNFs networks. Before treatment, the electric field could not go through the PEI-CNFs nanocomposites due to the negative permittivity, but the electric field could penetrate the nanocomposites after ultrasonic treatment. After testing the dielectric property of PEI-CNFs (ultrasonically treated), the researchers observed that the permittivity was positive and the resonance disappeared in the tested frequency range, indicating that the continuous 3D CNFs network could introduce negative permittivity.

3.4. Metacomposites with amorphous carbon as fillers

Cheng et al.[71] have reported the amorphous carbon-silicon nitride (C-Si_3N_4) metacomposites which were fabricated by a facile impregnation-carbonization process at low temperature. Negative permittivity (-600 to 0) consistent well with Drude model was obtained when the carbon content exceeded 13 wt%. Cheng et al.[72] also investigated how to tune the negative permittivity with different heat treatment temperatures (HTTs) and carbon contents in the C-Si_3N_4 metacomposites prepared by a feasible impregnation-pyrolysis method. They observed that negative permittivity was realized at high HTTs (≥850 °C). The negative permittivity agreed well with the Drude model. So the researchers believed that negative permittivity resulted from the low-frequency plasmon of free electrons in the conductive carbon networks.[51] A lot of free carriers in the C-Si_3N_4 metacomposites could offer the plasmonic state, and negative permittivity was achieved when the frequency of external electric field was below the plasma frequency of free electron.[17,73]

3.5. Metacomposites with two or more kinds of carbonaceous materials

Qian et al.[74] have fabricated the carbon nanotubes-graphene-phenolic resin (CNTs-GR-PR) metacomposites by using the mechanical pressing method, in order to investigate synergistic effects of CNTs on negative dielectric properties of GR-PR composites. The researchers

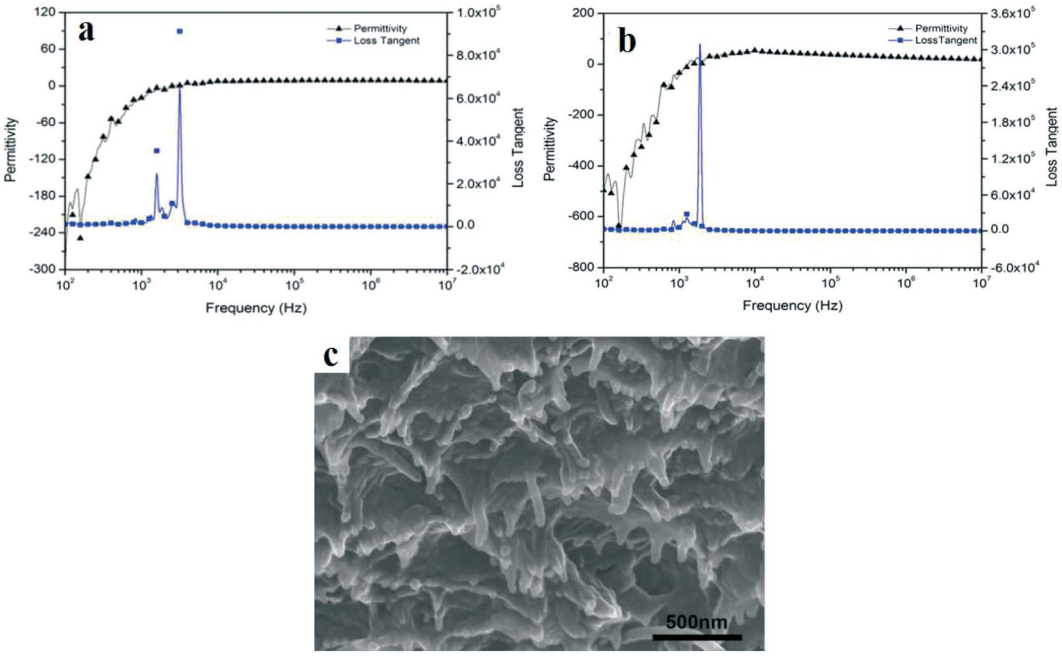

Fig. 4 Frequency dependence of dielectric permittivity and loss tangent of PI-MWCNTs composites with different MWCNTs contents: (a) 8.1 vol%, (b) 8.7 vol%, (c) SEM image of cross section of PI-MWCNTs composites with MWCNTs content of 8 vol%. Reprinted with permission.[69] Copyright 2015, AIP.

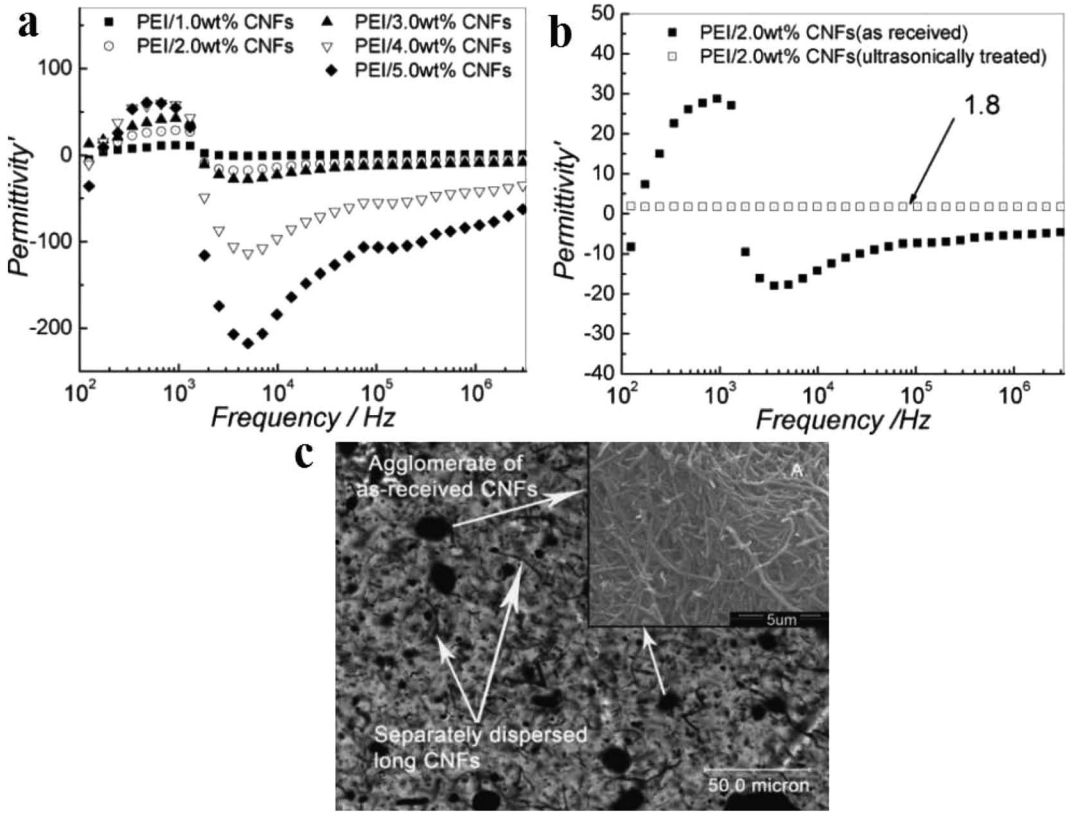

Fig. 5 Frequency dependence of the real permittivity of PEI-CNFs nanocomposites, (a) before the ultrasonic treatment, (b) after the ultrasonic treatment, (c) SEM image of PEI-CNFs (2 wt%, as-received) nanocomposites. Reprinted with permission.[18] Copyright 2009, Wiley.

found that negative permittivity appeared in CNTs-GR-PR composites when the total content of CNTs and GR was 6.6 wt%. However, negative permittivity in GR-PR composites began to appear when GR content was 10 wt%. So the addition of CNTs in GR-PR composites is beneficial for the realization of negative permittivity.

4. The potential applications of metacomposites

4.1. Applications in the field of electromagnetic wave absorption

Metacomposites show great potential applications in the field of electromagnetic wave absorption. Electromagnetic wave absorbing materials have attracted much attention because they can greatly reduce the chance of an aircraft being discovered by radar and thus improve its survivability. According to the absorption mechanism, electromagnetic wave absorbing materials can be classified into magnetic wave absorbing materials, electronic wave absorbing materials and chiral absorbing materials, etc.[75] Metacomposites with carbon materials as fillers mainly rely on good conductivity and high dielectric loss to absorb the energy of electromagnetic waves, exhibiting advantages of light weight and easy adjustment.[76]

4.2. Applications in the area of improving the performance of the antenna

In addition, metacomposites are often used to improve the performance of the antenna, such as improving the radiation efficiency of the antenna, reducing the size of the antenna structure, broadening the operating frequency band of the antenna, and achieving antenna direction control. In the metacomposites, the appearance of negative permittivity is often accompanied by the appearance of an inductor in the equivalent circuit model, so metacomposites exhibit an inductive characteristic. By covering the antenna with metacomposites, the radiation impedance of the antenna possibly is converted from a capacitive characteristic to an inductive characteristic, which makes it easier for the antenna to achieve impedance matching, thereby improving the radiation efficiency of the antenna.[77]

5. Conclusions and Perspective

In conclusion, the review about negative permittivity in metacomposites filled with carbon nanostructures was introduced in this article. The main models which were the fundamental theories for negative permittivity were discussed in detail. And the present reports on carbon nanofillers metacomposites with negative permittivity were introduced. The mechanisms for negative permittivity from different metacomposites were also presented. In the metacomposites with carbon nanofillers, the microstructures and compositions of conductive phases played an important role in the negative permittivity. But how to make carbon nanofillers dispersed more evenly in the matrix is still a challenge. Besides, due to the lack of magnetic properties in metacomposites compared with common metamaterials, applications of these metacomposites are limited in some fields like computer memory, magnetoresistance sensors and magnetic recording systems.[78–82]

The negative permittivity of metacomposites possibly are tuned by surface modification of carbon materials. Although the research on metacomposites is on the starting stage, the applications of metacomposites in electromagnetic interference absorbing and shielding, sensors, machine intelligence and other fields are potential.[83–85] In addition, the preparation of metacomposites also provides a novel idea to design the next-generation metamaterials.

Conflict of interest

There are no conflicts to declare.

Acknowledgments

We are grateful to the National Nature Science Foundation of China (No. 51672162), State Education Ministry and State Key Laboratory of New Ceramic and Fine Processing Tsinghua University (No. KF201606), the Fundamental Research Funds of Shandong University (No.2017JC035).

References

1 H. Gu, J. Guo, S. Wei and Z. Guo, *J. Appl. Polym. Sci.*, 2013, **130**, 2238–2244.
2 F. Capolino, *Theory and phenomena of metamaterials*, CRC press, 2009.
3 V. G. Veselago, *Sov. Phys. Usp.*, 1968, **10**, 509–514.
4 A. A. Houck, J. B. Brock and I. L. Chuang, *Phys. Rev. Lett.*, 2003, **90**, 137401.
5 N. Fang, H. Lee, C. Sun and X. Zhang, *Science*, 2005, **308**, 534–537.
6 J. B. Pendry, D. Schurig and D. R. Smith, *Science*, 2006, **312**, 1780–1782.
7 V. M. Shalaev, *Nature Photon.*, 2007, **1**, 41–48.
8 D. Schurig, J. J. Mock, B. J. Justice, S. A. Cummer, J. B. Pendry, A. F. Starr and D. R. Smith, *Science*, 2006, **314**, 977–980.
9 H. J. Lezec, J. A. Dionne and H. A. Atwater, *Science*, 2007, **316**, 430–432.
10 J. B. Pendry, A. J. Holden, W. J. Stewart and I. Youngs, *Phys. Rev. Lett.*, 1996, **76**, 4773–4776.
11 R. Ziolkowski and E. Heyman, *Phys. Rev. E*, 2001, **64**, 056625.
12 K. Sun, P. Xie, Z. Wang, T. Su, Q. Shao, J. Ryu, X. Zhang, J. Guo, A. Shankar, J. Li, R. Fan, D. Cao and Z. Guo, *Polymer*, 2017, **125**, 50–57.
13 J. Pendry, *Phys. Rev. Lett.*, 2000, **85**, 3966.
14 B. Wang, K. Teo, T. Nishino, W. Yerazunis, J. Barnwell and J. Zhang, *Appl. Phys. Lett.*, 2011, **98**, 254101.
15 M. Freire, R. Marques and L. Jelinek, *Appl. Phys. Lett.*, 2008, **93**, 231108.
16 J. Zhu, S. Wei, L. Zhang, Y. Mao, J. Ryu, A. Karki, D. Young and Z. Guo, *J. Mater. Chem.*, 2011, **21**, 342–348.
17 J. Zhu, S. Wei, L. Zhang, Y. Mao, J. Ryu, P. Mavinakuli, A. Karki, D. Young and Z. Guo, *J. Phys. Chem. C*, 2010, **114**, 16335–16342.
18 B. Li, G. Sui and W. Zhong, *Adv. Mater.*, 2009, **21**, 4176–4180.
19 Z. Shi, R. Fan, Z. Zhang, L. Qian, M. Gao, M. Zhang, L. Zheng, X. Zhang and L. Yin, *Adv. Mater.*, 2012, **24**, 2349–2352.
20 H. Chen, *J. Mater. Chem.*, 2011, **21**, 6452–6463.
21 C. D. Liu, S. N. Lee, C. H. Ho, J. L. Han and K. H. Hsieh, *J. Phys. Chem. C*, 2008, **112**, 15956–15960.
22 R. Aepuru, B. V. B. Rao, S. N. Kale and H. S. Panda, *Mater. Chem. Phys.*, 2015, **167**, 61–69.
23 A. J. Holden, *Photonics Nanostruct. Fundam. Appl.*, 2005, **3**, 96–99.
24 X. Zhang, X. Yan, Q. He, H. Wei, J. Long, J. Guo, H. Gu, J. Yu, J. Liu, D. Ding, L. Sun, S. Wei and Z. Guo, *ACS Appl. Mater. Interfaces*, 2015, **7**, 6125–6138.
25 J. Pendry, L. Martin-Moreno and F. Garcia-Vidal, *Science*, 2004, **305**, 847–848.
26 M. Dressel and G. Gruener, *Electrodynamics of solids: optical properties of electrons in matter*, Cambridge University Press, Cambridge, 2002.
27 A. McAlister and E. Stern, *Phys. Rev.*, 1963, **132**, 1599.
28 S. Nagel and S. Schnatterly, *Phys. Rev. B*, 1974, **9**, 1299.
29 P. Johnson and R. Christy, *Phys. Rev. B*, 1972, **6**, 4370–4379.
30 J. McMahon, S. Gray and G. Schatz, *Phys. Rev. Lett.*, 2009, **103**, 097403.
31 M. Rashidi-Huyeh and B. Palpant, *Phys. Rev. B*, 2006, **74**, 075405.
32 S. Enoch, G. Tayeb, P. Sabouroux, N. Guerin and P. Vincent, *Phys. Rev. Lett.*, 2002, **89**, 213902.
33 S. Ramakrishna and T. Grzegorczyk, *Physics and applications of negative refractive index materials,* CRC press, 2008.
34 T. Tsutaoka, H. Massango, T. Kasagi, S. Yamamoto and K. Hatakeyama, *Appl. Phys. Lett.*, 2016, **108**, 191904.
35 K. Yan, R. Fan, M. Chen, K. Sun, L. Yin, H. L. S. Pan and M. Yu, *J. Alloy. Compd.*, 2015, **628**, 429–432.
36 H. Yan, C. Zhao, K. Wang, L. Deng, M. Ma and G. Xu, *Appl. Phys. Lett.*, 2013, **102**, 062904.
37 X. Yao, X. Kou, J. Qiu and M. Moloney, *J. Phys. Chem. C*, 2016, **120**, 4937–4944.
38 X. Yao, X. Kou, J. Qiu and M. Moloney, *RSC Adv.*, 2016, **6**, 35378–35386.
39 Z. Guo, L. Henry, V. Palshin and E. Podlaha, *J. Mater. Chem.*, 2006, **16**, 1772–1777.
40 C. Castro, J. Ramos, A. Millán, C. Gonzalez and F. Palacio, *Chem. Mater.*, 2000, **12**, 3681–3688.
41 V. Yong and H. Hahn, *Nanotechnology*, 2004, **15**, 1338.
42 J. Mack, L. Viculis, A. Ali, R. Luoh, G. Yang, H. Hahn, F. Ko and R. Kaner, *Adv. Mater.*, 2005, **17**, 77–80.
43 G. Sandí, H. Joachin, R. Kizilel, S. Seifert and K. Carrado, *Chem. Mater.*, 2003, **15**, 838–843.
44 J. Zhu, S. Wei, J. Ryu, M. Budhathoki, G. Liang and Z. Guo, *J. Mater. Chem.*, 2010, **20**, 4937–4948.
45 J. Zhu, S. Wei, J. Ryu, L. Sun, Z. Luo and Z. Guo, *ACS Appl. Mater. Interfaces*, 2010, **2**, 2100–2107.
46 J. Zhu, S. Wei, X. Chen, A. Karki, D. Rutman, D. Young and Z. Guo, *J. Phys. Chem. C*, 2010, **114**, 8844–8850.
47 Z. Guo, S. Lee, H. Kim, S. Park, H. Hahn, A. Karki and D. Young, *Acta Mater.*, 2009, **57**, 267–277.
48 Z. Guo, S. Park, H. Hahn, S. Wei, M. Modlovan, A. Karki and D. Young, *J. Appl. Phys.*, 2007, **101**, 09M511.
49 Z. Guo, H. Hahn, H. Lin, A. Karki and D. Young, *J. Appl. Phys.*, 2008, **104**, 014314.
50 S. Liu, L. Wei, L. Hao, N. Fang, M. Chang, R. Xu, Y. Yang and Y. Chen, *ACS Nano*, 2009, **3**, 3891–3902.
51 T. Tsutaoka, T. Kasagi, S. Yamamoto and K. Hatakeyama, *Appl. Phys. Lett.*, 2013, **102**, 181904.
52 A. Balandin, S. Ghosh, W. Bao, I. Calizo, D. Teweldebrhan, F. Miao and C. Lau, *Nano Lett.*, 2008, **8**, 902–907.
53 C. Lee, X. Wei, J. Kysar and J. Hone, *Science*, 2008, **321**, 385–388.
54 S. Stankovich, D. Dikin, P. Piner, K. Kohlhaas, A. Kleinhammes, Y. Jia, Y. Wu, S. Nguyen and R. Ruoff, *Carbon*, 2007, **45**, 1558–1565.
55 S. Morozov, K. Novoselov, M. Katsnelson, F. Schedin, D. Elias, J. Jaszczak and A. Geim, *Phys. Rev. Lett.*, 2008, **100**, 016602.
56 Q. He, T. Yuan, Z. Luo, N. Haldolaarachchige, D. Young, S. Wei and Z. Guo, *Chem. Commun.*, 2013, **49**, 2679–2681.
57 M. Chen, H. Qu, J. Zhu, Z. Luo, A. Khasanov, A. Kucknoor, N. Haldolaarachchige, D. Young, S. Wei and Z. Guo, *Polymer*, 2012, **53**, 4501–4511.
58 H. Wei, X. Yan, S. Wu, Z. Luo, S. Wei and Z. Guo, *J. Phys. Chem. C*, 2012, **116**, 25052–25064.
59 X. Zhang, Q. He and H. Gu, *J. Mater. Chem. C*, 2013, **1**, 2886–2899.
60 S. Nosheen, M. Raza, S. Alam, M. Irfan, A. Iftikhar, F. Iftikhar, B. Waseem, Z. Abbas and B. Soomro, *Arab. J. Sci. Eng.*, 2017, **42**, 193–199.
61 W. Zhao, J. Kong, H. Liu, Q. Zhuang, J. Gu and Z. Guo, *Nanoscale*, 2016, **8**, 19984–19993.
62 K. Zarasvand and H. Golestanian, *Compos. Sci. Technol.*, 2017, **139**, 117–126.
63 H. Wu, Y. Zhang, R. Yin, W. Zhao, X. Li and L. Qian, *Adv. Compos. Hybrid Mater.*, 2018, **1**, 168–176.
64 R. Yin, H. Wu, K. Sun, X. Li, C. Yan, W. Zhao, Z. Guo and L. Qian, *J. Phys. Chem. C*, 2018, **122**, 1791–1799.
65 J. Zhu, Z. Luo, S. Wu, N. Haldolaarachchige, D. Young, S. Wei and Z. Guo, *J. Mater. Chem.*, 2012, **22**, 835.
66 H. Wu, Y. Qi, Z. Wang, W. Zhao, X. Li and L. Qian, *Compos. Sci. Technol.*, 2017, **151**, 79–84.
67 H. Wu, R. Yin, L. Qian and Z. Zhang, *Mater. Design*, 2017, **117**, 18–23.
68 C. Cheng, R. Fan, Y. Ren, T. Ding, L. Qian, J. Guo, X. Li, L. An, Y. Lei and Y. Yin, *Nanoscale*, 2017, **9**, 5779–5787.

69 Y. Sun, J. Wang, S. Qi, G. Tian and D. Wu, *Appl. Phys. Lett.*, 2015, **107**, 012905.

70 J. Zhu, S. Wei, J. Ryu and Z. Guo, *J. Phys. Chem. C*, 2011, **115**, 13215–13222.

71 C. Cheng, K. Yan, R. Fan, L. Qian, Z. Zhang, K. Sun and M. Chen, *Carbon*, 2016, **96**, 678–684.

72 C. Cheng, R. Fan, Z. Wang, Q. Shao, X. Guo, P. Xie, Y. Yin, Y. Zhang, L. An, Y. Lei, J. Ryu, A. Shankar and Z. Guo, *Carbon*, 2017, **125**, 103–112.

73 Z. Shi, R. Fan, K. Yan, K. Sun, M. Zhang, C. Wang, X. Liu and X. Zhang, *Adv. Funct. Mater.*, 2013, **23**, 4123–4132.

74 H. Wu, R. Yin, Y. Zhang, Z. Wang, P. Xie and L. Qian, *J. Phys. Chem. C*, 2017, **121**, 12037–12045.

75 J. Zhong, PhD thesis, University of Electronic Science and Technology of China, 2013.

76 Y. He, PhD thesis, Zhejiang University, 2013.

77 J. Ye, PhD thesis, Nanjing University of Aeronautics and Astronautics, 2012.

78 H. Gu, J. Guo, H. Wei, S. Guo, J. Liu, Y. Huang, M. Khan, X. Wang, D. Young, S. Wei and Z. Guo, *Adv. Mater.*, 2015, **27**, 6277–6282.

79 P. Grünberg, *Rev. Mod. Phys.*, 2008, **80**, 1531.

80 W. Gallagher and S. Parkin, *IBM J. Res. Dev.*, 2006, **50**, 5–23.

81 R. Freitas and W. Wilcke, *IBM J. Res. Dev.*, 2008, **52**, 439–447.

82 D. Graham, H. Ferreir and P. Freitas, *Trends. Biotechnol.*, 2004, **22**, 455–462.

83 C. Alippi, *CAAI Trans. Intel. Tech.*, 2016, **1**, 1–3.

84 H. Jin, Q. Chen, Z. Chen, Y. Hu and J. Zhang, *CAAI Trans. Intel. Tech.*, 2016, **1**, 104–113.

85 X. Zhang, H. Gao, M. Guo, G. Li, Y. Liu and D. Li, *CAAI Trans. Intel. Tech.*, 2016, **1**, 4–13.